Supporting Information

Supramolecular J-aggregates of aza-BODIPY by Steric and π-π Interactions for NIR-II Phototheranostic

Youliang Tian, Dalong Yin, Quan Cheng, Huiping Dang, Changchang Teng, Lifeng Yan *

Department of Hepatobiliary Surgery, The First Affiliated Hospital, Division of Life Sciences and Medicine, and Department of Chemical Physics, University of Science and Technology of China, Hefei, 230026, China

Materials and apparatus.

Triphenylamine, acetyl chloride, anhydrous aluminium chloride, 4-methoxybenzaldehyde, 4-methoxyphenylboronic acid, 5-bromo-2-thiophenealdehyde, [1,1′-bis(diphenylphosphino)-ferrocene]palladium(II) dichloride dichloromethane complex, nitromethane, 1,8-diazabicyclo[5.4.0]undec-7-ene (DBU), diethylamine, ammonium acetate, N,N-diisopropylethylamine, boron (tri) fluoride etherate ($BF_3 \cdot C_2H_5OC_2H_5$) was purchased from Aladdin Corporation (China). Methyl thiazolyl tetrazolium (MTT), fluorescein diacetate (FDA), and propidium iodide (PI) were obtained from Sangon Corporation, China. Annexin V-FITC Apoptosis Detection Kit was purchased from Beyotime Biotechnology Corporation. All the solvents used in column chromatography come from J&K (China).

^1H NMR and ^{13}C NMR spectra were scanned on Bruker AC 400/500 spectrometer with chloroform-d ($CDCl_3$) as solvent. High resolution or MALDI-TOF mass spectral analysis was performed on Waters XEVO G2 Q-TOF (Waters Corporation) or Atouflex Speed (Bruker Corporation). UV-vis absorption spectra were recorded by an UV-1700PC ultraviolet

spectrophotometer. The NIR fluorescence emission spectra were recorded using an Edinburgh FLS1000 fluorescence spectrophotometer equipped with an 808 nm laser diode. The size and morphology of dyes aggregates or J-NPs were measured by transmission electron microscope (TEM, JEM-2100) and atomic force microscope (AFM, Nanoscope Ⅴ). The particle sizes and their distributions were detected by a zeta-potential analyzer with dynamic laser light scattering (DLS) by a Malvern Zetasizer Nano ZS90 machine containing a He–Ne laser. The temperature variation curves of micelle were recorded by an Atest thermometer (DT-847UD). Fluorescence imaging *in vitro* was carried out by using a fluorescence microscope (IX71, Olympus). The whole-body NIR-II fluorescence imaging was performed by using an InGaAs camera (C-Red 2). The thermal imaging of mice was detected by an infrared thermal camera (Fotric 225S, ZXF Laboratorise, LLC).

293T and HepG2 cells from ATCC (American Type Culture Collection) were cultured in Dulbecco's Modified Eagle's medium (DMEM, Hyclone, USA) with 10% fetal bovine serum (FBS, ExCell Bio, Shanghai, China) at 37 ^{o}C with 5% CO_2. 4T1 cancer cells from ATCC (American Type Culture Collection) were cultured in RPMI（1640）with 10% fetal bovine serum (FBS, ExCell Bio, Shanghai, China) under the same condition.

Preparation and characterization of dye-assemblies

The dispersion liquid containing the concentration of the same dye was prepared by adjusting the ratio of THF to water. Typically, a THF solution of aza-BODIPY dyes (dye 1 and dye 2) was added deionized water and waggled rapidly about 30 s. After standing for 10 minutes, the samples were used for further testing.

Absorption and emission spectra: Dyes dispersion liquid (20 μM) containing different ratios of THF and water (0, 10%, 20%, 30%, 40%, 50%, 60%, 70%, 80%, 90%) was prepared, the

absorption and emission spectra of the obtained samples were recorded.

Atomic force microscopy (AFM): The samples were prepared by dip coating 20 μL of BODIPY dye-assemblies (20 μM) in THF/H_2O mixture (water fractions was 90%) onto freshly cleaved mica surfaces. Then, atomic force microscope (AFM, Nanoscope Ⅴ; Digital Instruments) was used to observe the morphology and thickness of aggregates.

Theoretical calculations

All the calculations were based on density functional theory (DFT) with B3LYP functional and 6-31G (d) basis set. Frontier molecular orbitals and their orbital energies were calculated with the TD-DFT methods based on the optimized ground state geometry. All these calculations were performed with Gaussian 09W[1].

Preparation and character of micelle

Amphiphilic polypeptide $POEGMA_{23}$-$PAsp_{20}$ was synthesized according to the previous literature method [2, 3]. 5 mg dye 2 and 100 mg $POEGMA_{23}$-$PAsp_{20}$ polymer was ultrasonically dissolved in 4 mL THF, then 16 mL of deionized water was poured into under vigorous stirring, the mixture was stirred for 30 min. Then, the solution was then dialyzed against ultrapure water for 24 h in a 10000 molecular weight dialysis bag. The aqueous solution was further centrifuged with a centrifugal-filter (MWCO = 10 kDa) at 6000 r for 15 min and filtered through a 0.22 μm filter for cell and animal experiments.

Stability characterization of micelles

Stability under different acidity conditions: 1 mM J-aggregation NPs was diluted into different pH value (7.4, 6.5, 5.5, 4.5) buffer solution (dye concentration: 30 μM). Then the absorption spectra, DLS, fluorescence behavior of micelles under different acidity conditions was observed. In addition, the absorption and fluorescence of J-NPs in the saline (0.9 % NaCl),

PBS, and FBS were also observed.

The resistance to photobleaching and H_2O_2

In order to evaluate the resistance to photobleaching, the micelles (30 μM) were exposed to a 915 nm laser (1 W/cm^2) for 20 minutes, and the absorption spectrum was recorded at five-minute intervals. After that, the DLS, fluorescence behavior of micelles was further observed. Similarly, the absorption spectra, DLS, fluorescence behavior were explored after the J-NPs were incubated with hydrogen peroxide (200 μM). As a comparison, the tolerance of ICG to hydrogen peroxide and photobleaching was also tested.

Photothermal effect and photothermal conversion efficiency calculation of J-NPs

First of all, in order to evaluate the effect of concentration on photothermal behavior of nanoparticles, pure water and different concentration of J-NPs (5 μM, 10 μM, 20 μM, 30 μM) were prepared and irradiated by 915 nm laser with a power density of 1.0 W/cm^2 for 5 min. The temperature changes were monitored by an Atest thermometer (DT-847UD). Then, the effect of power density on temperature was discussed. J-NPs (30 μM) were irradiated by 915 nm laser at different power densities (0.2 W/cm^2, 0.4 W/cm^2, 0.6 W/cm^2, 0.8 W/cm^2, 1.0 W/cm^2). To measure the photothermal conversion efficiency, J-NPs (30 μM) were exposed to 915 nm irradiation at 1 W/cm^2 for 10 min, and then the solution was cooled down to room temperature. The temperature of the solution was recorded at an interval of 15 s during this process. The photothermal conversion efficiency (η) was measured according to the reported method [4].

$$\eta = \frac{hs(T_{Max} - T_{Surr}) - Q_{Dis}}{I\left(1 - 10^{-A_{915}}\right)}$$

h is the heat transfer coefficient; s is the surface area of the container. Q_{Dis} represents heat dissipated from the laser mediated by the solvent and container. I is the laser power and A is the

absorbance at 915 nm.

$$hs = \frac{mC_{water}}{\tau_s}$$

m is the mass of the solution containing the photoactive material, C is the specific heat capacity of the solution (C_{water}= 4.2 J/(g•°C)), and τ_s is the associated time constant.

$$t = -\tau_s In(\theta)$$

θ is a dimensionless parameter, known as the driving force temperature

$$\theta = \frac{T - T_{Surr}}{T_{Max} - T_{Surr}}$$

T_{Max} and T_{Surr} are the maximum steady-state temperature and the environmental temperature, respectively. Besides, the photothermal stability of J-aggregation nanoparticles (30 μM) was measured by six cycles of heating-cooling processes (915 nm, 1 W/cm^2).

Tumor model

Female Balb/c mice (5 weeks old, Beijing Vital River Laboratory Animal Technology Co., Ltd.) cared under protocols approved by the University of Science and Technology of China Animal Care and Use Committee (No. USTCACUC1801006)..

In order to build the tumor model, mice were subcutaneously injected with 4T1 cells (about 10^6 per tumor) in the right side for NIR-II fluorescence imaging assay, or both sides on the back for *in vivo* phototherapy effect. The mice were further treated when the volume of the tumor reaches about 100 mm^3.

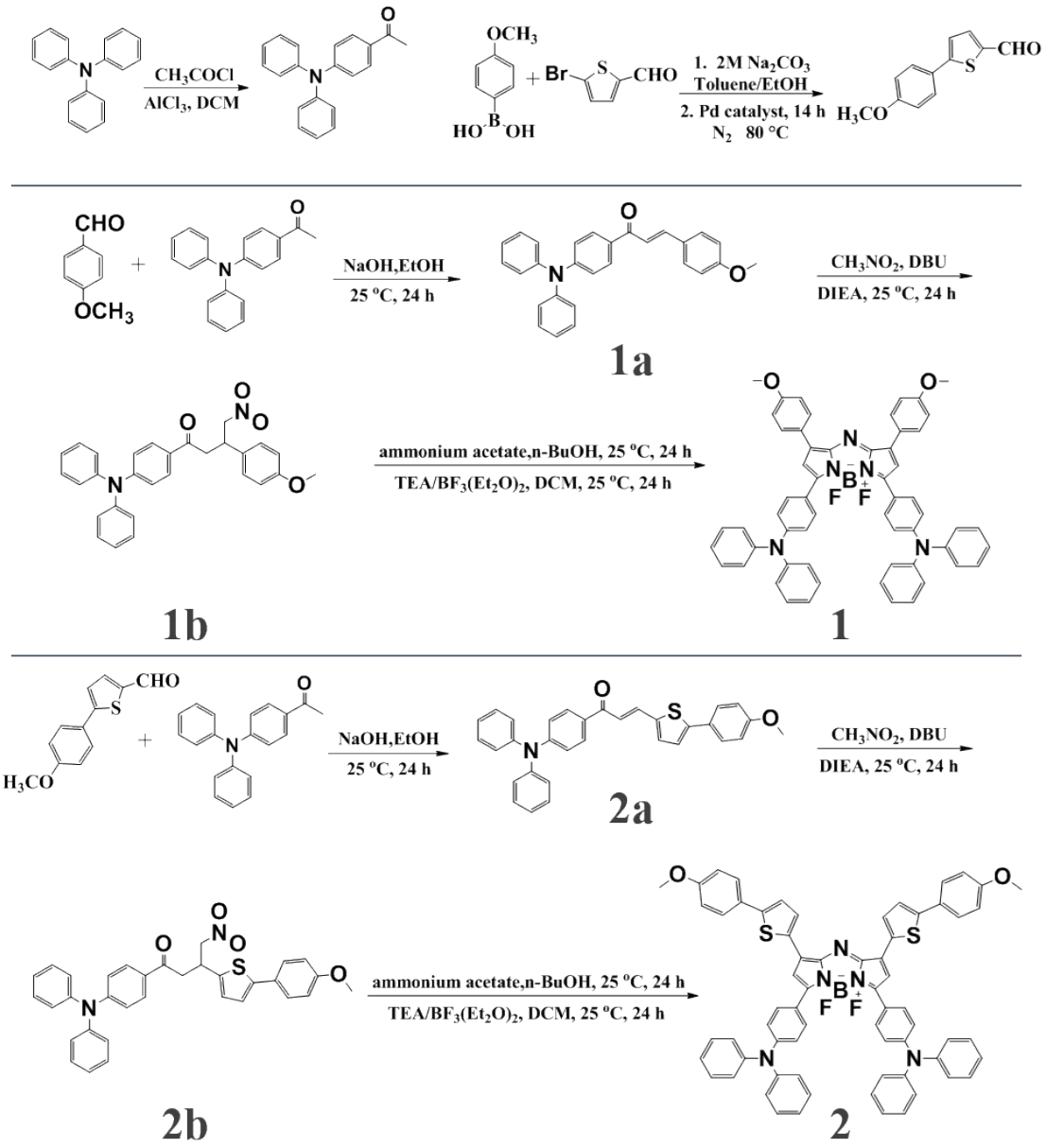

Figure S1. The synthetic routes of dye 1 and 2.

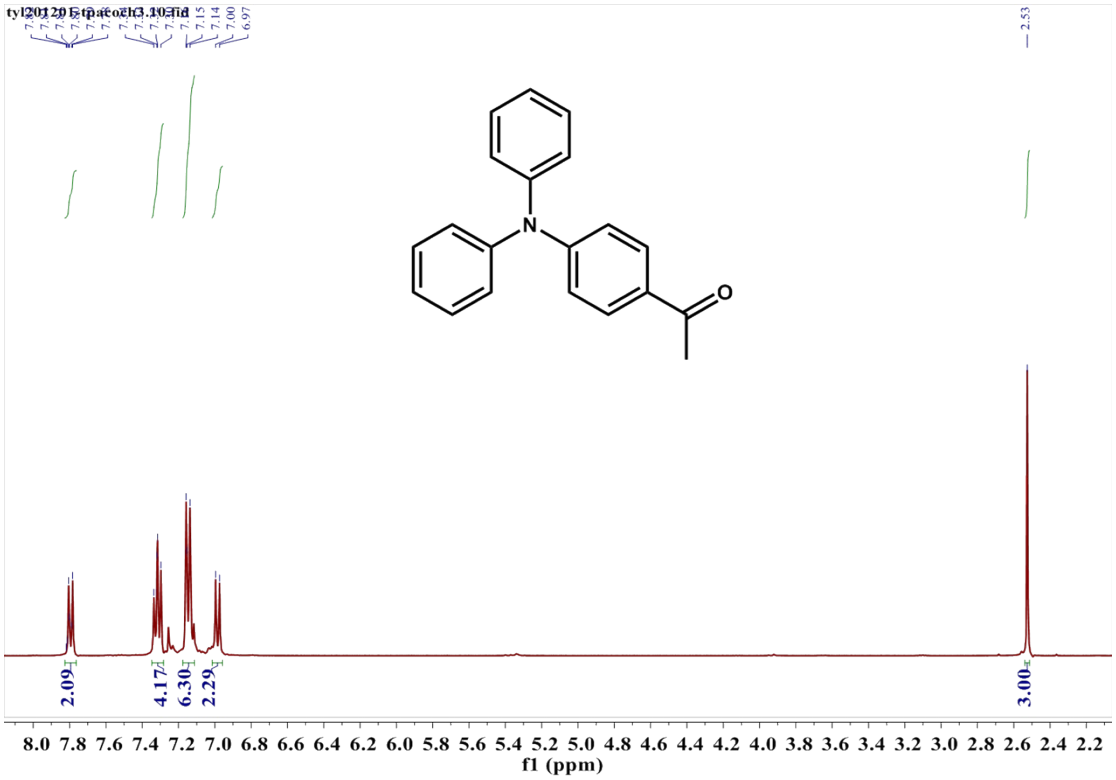

Figure S2. ^{1}H NMR spectrum of 1-(4-(N,N-diphenylamino)phenyl)ethanone in $CDCl_3$.

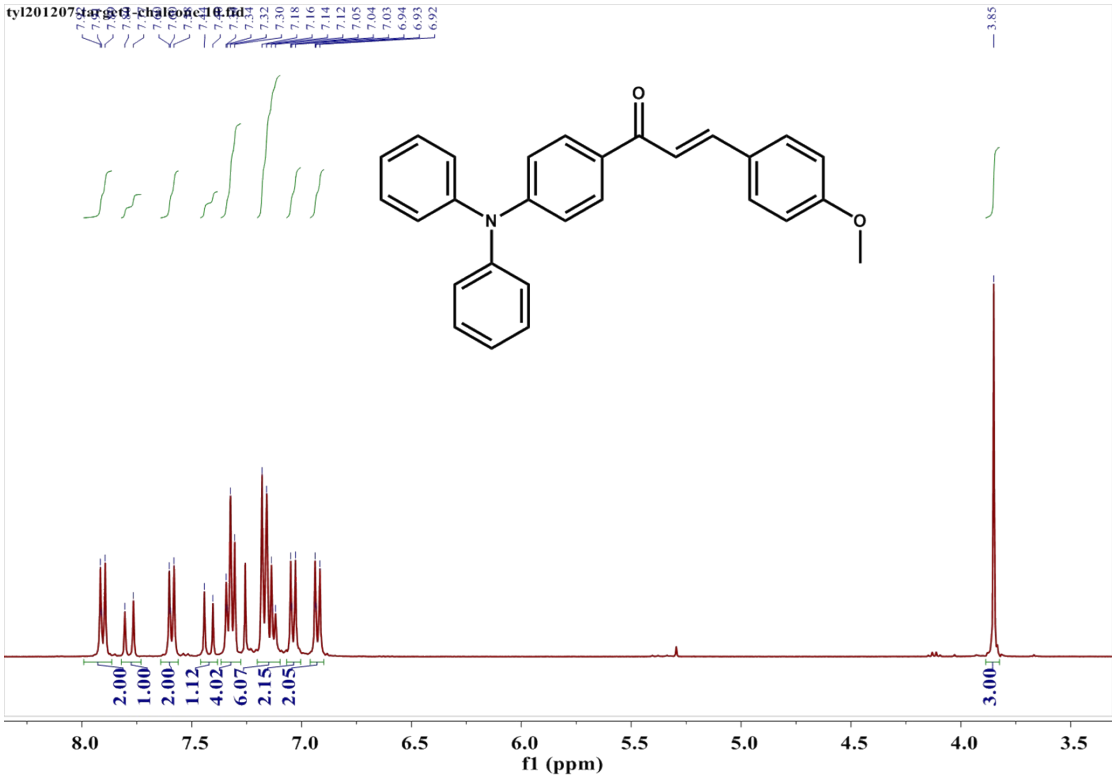

Figure S3. ^{1}H NMR spectrum of 1a in $CDCl_3$.

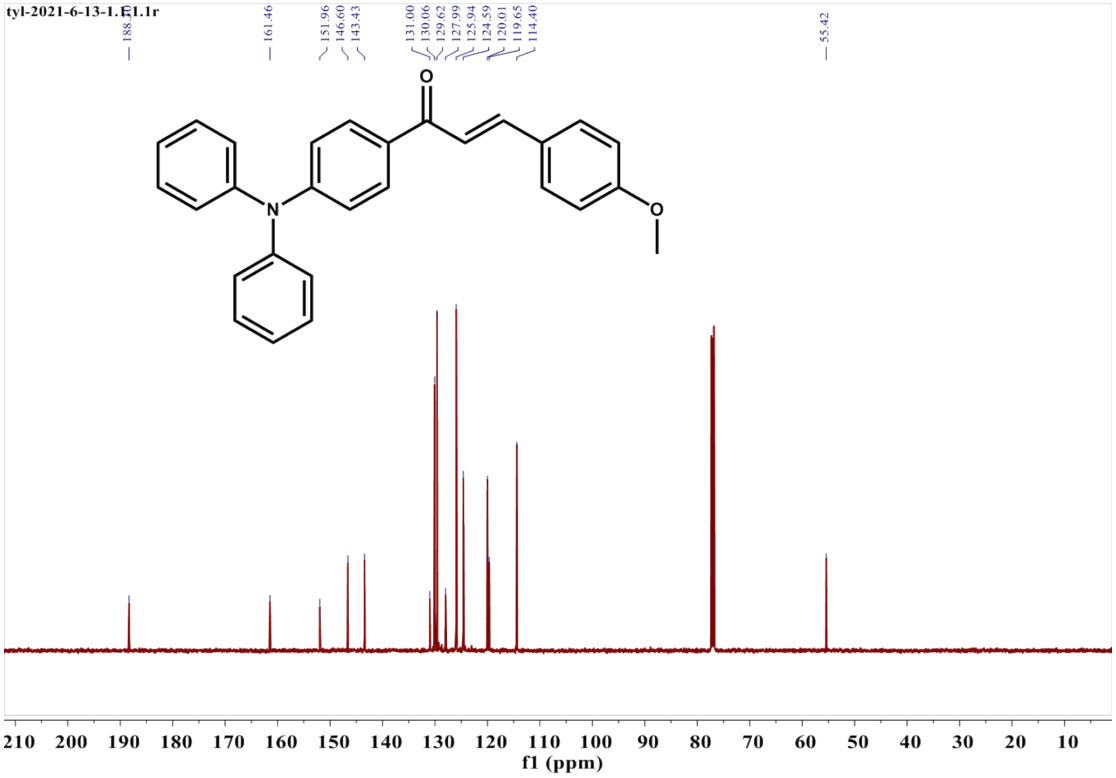

Figure S4. ^{13}C NMR spectrum of 1a in $CDCl_3$.

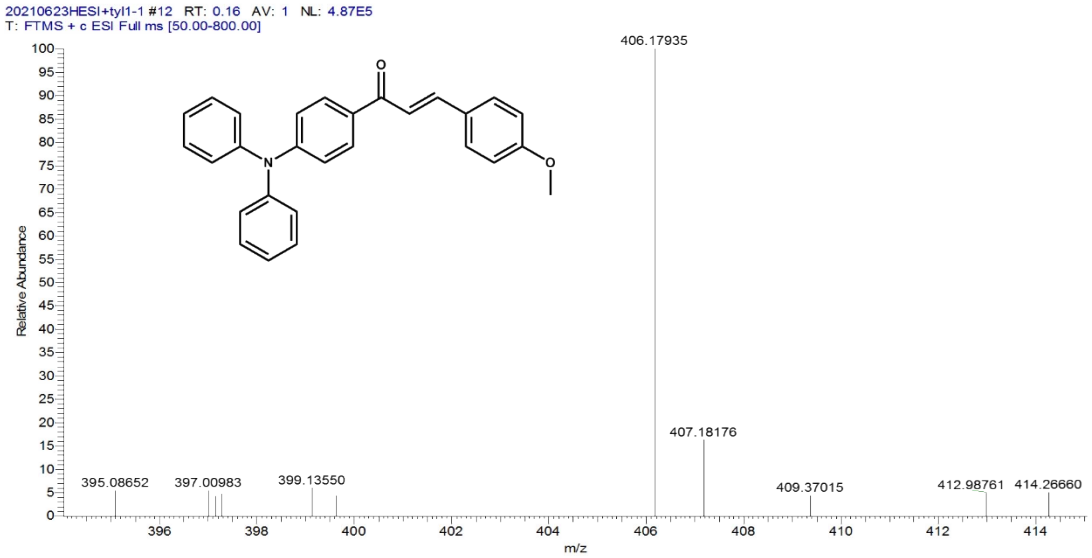

Figure S5. HR-MS spectrum of compound 1a.

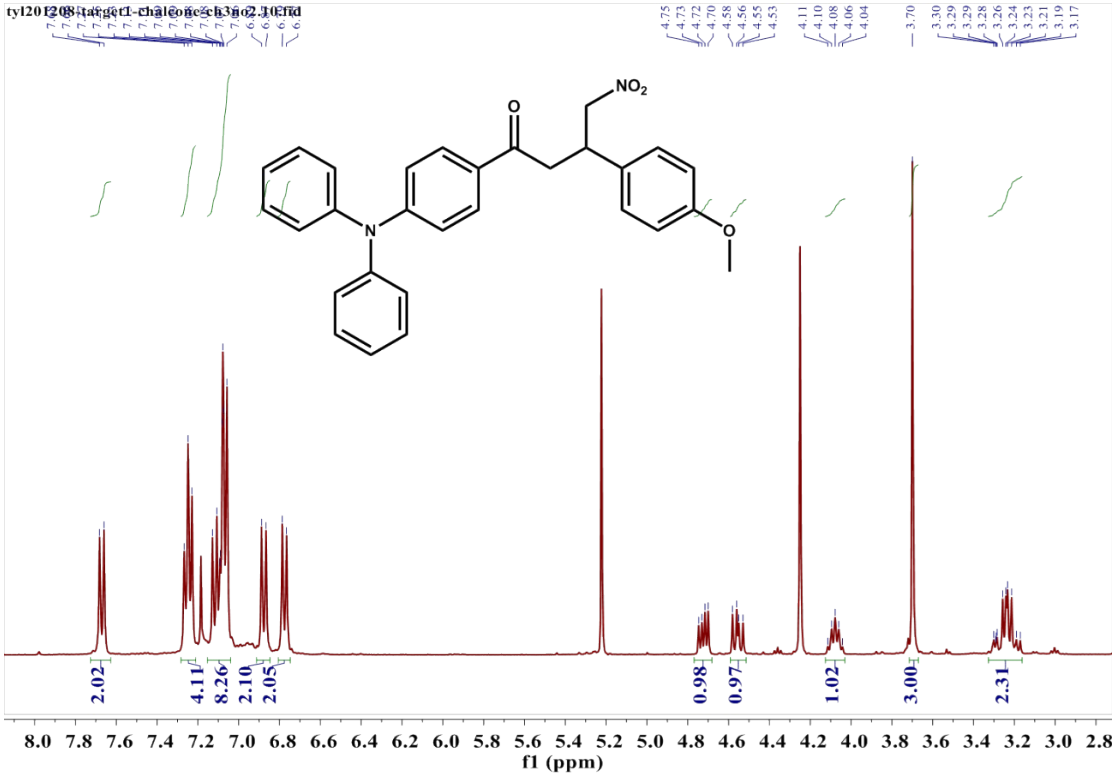

Figure S6. ^{1}H NMR spectrum of 1b in $CDCl_3$.

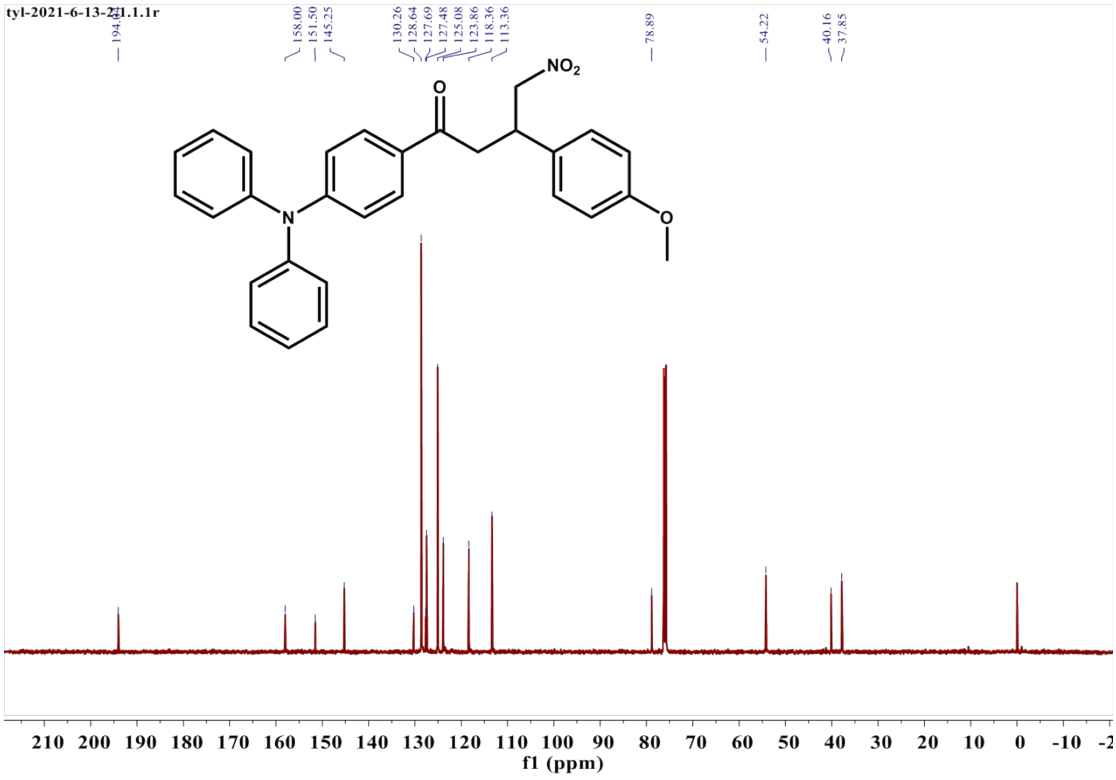

Figure S7. ^{13}C NMR spectrum of 1b in $CDCl_3$.

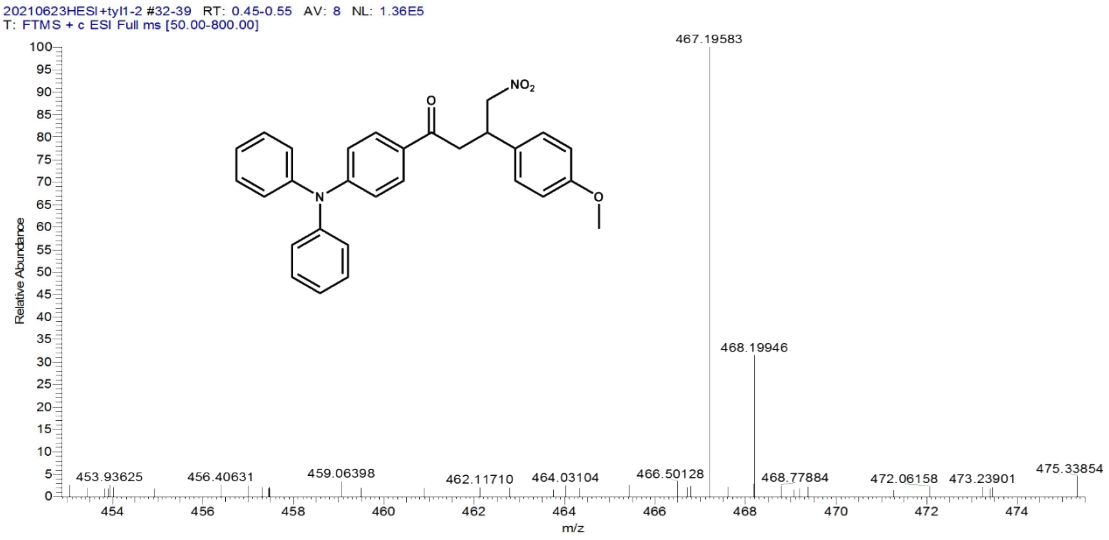

Figure S8. HR-MS spectrum of 1b.

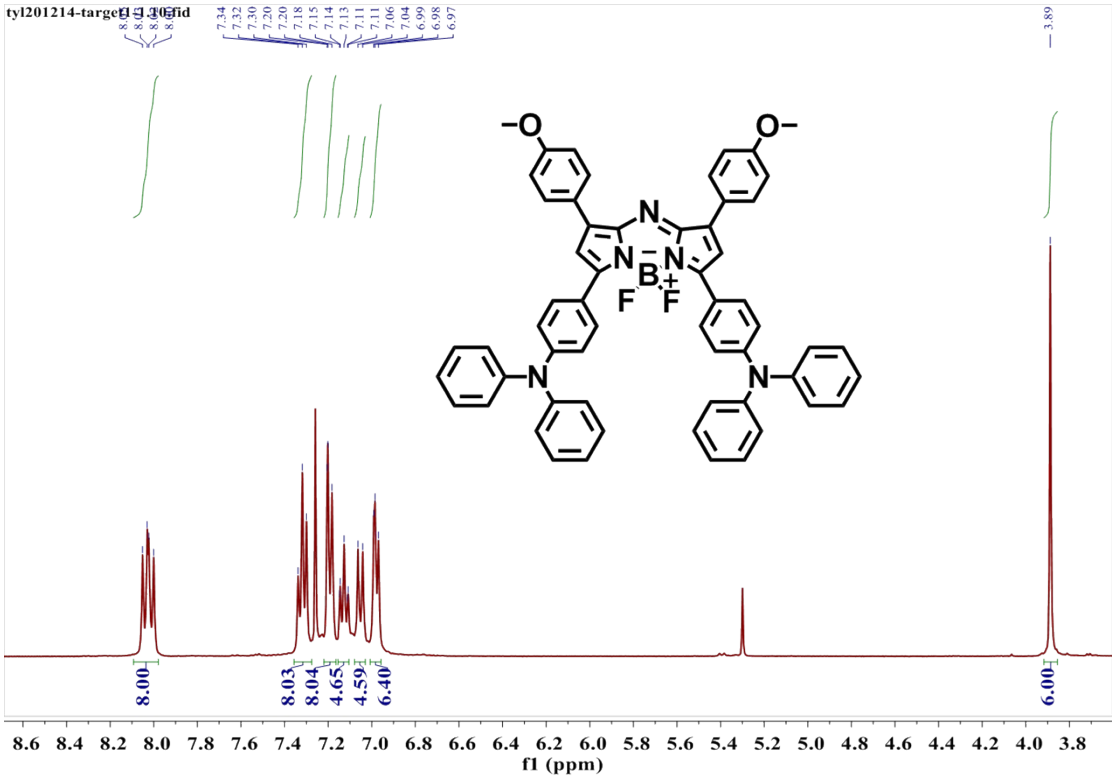

Figure S9. ^{1}H NMR spectrum of dye 1 in $CDCl_3$.

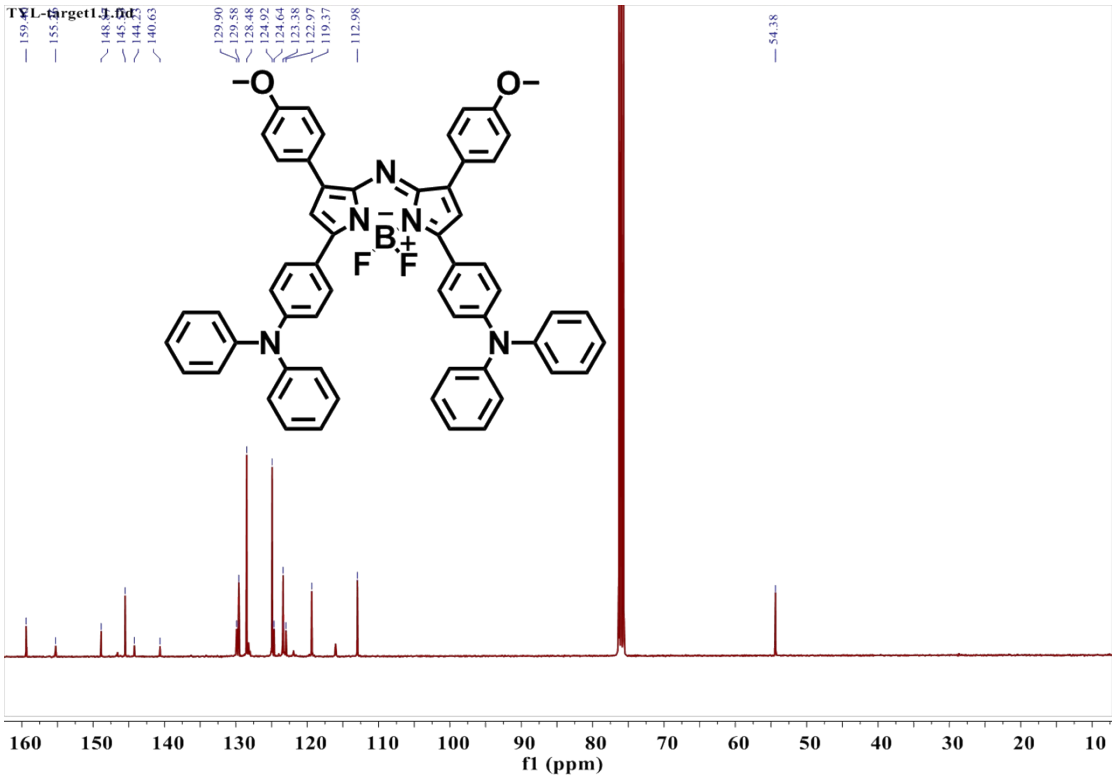

Figure S10. ^{13}C NMR spectrum of dye 1 in $CDCl_3$.

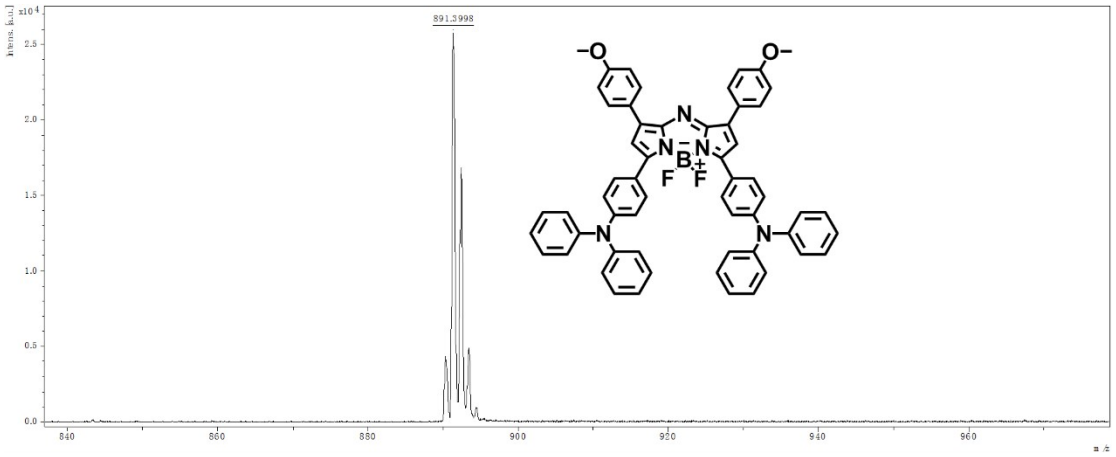

Figure S11. MALDI-TOF-MS spectrum of dye 1.

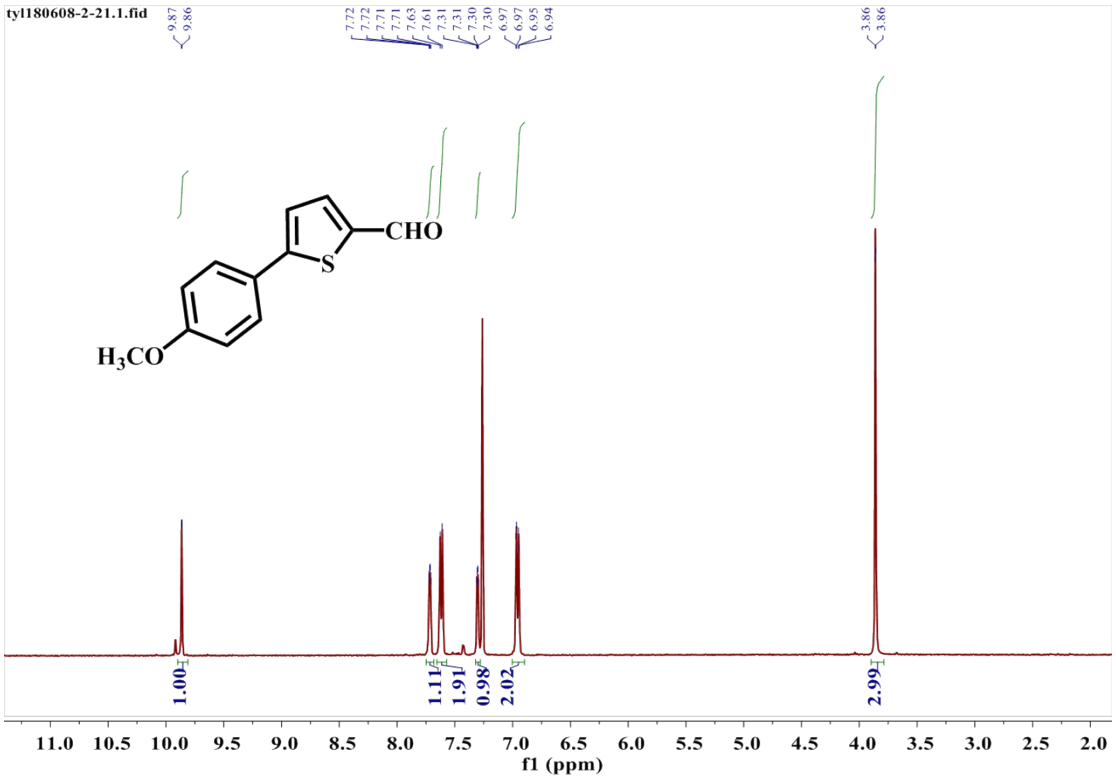

Figure S12. ^{1}H NMR spectrum of 5-(4-methoxyphenyl)thiophene-2-carbaldehyde in $CDCl_3$

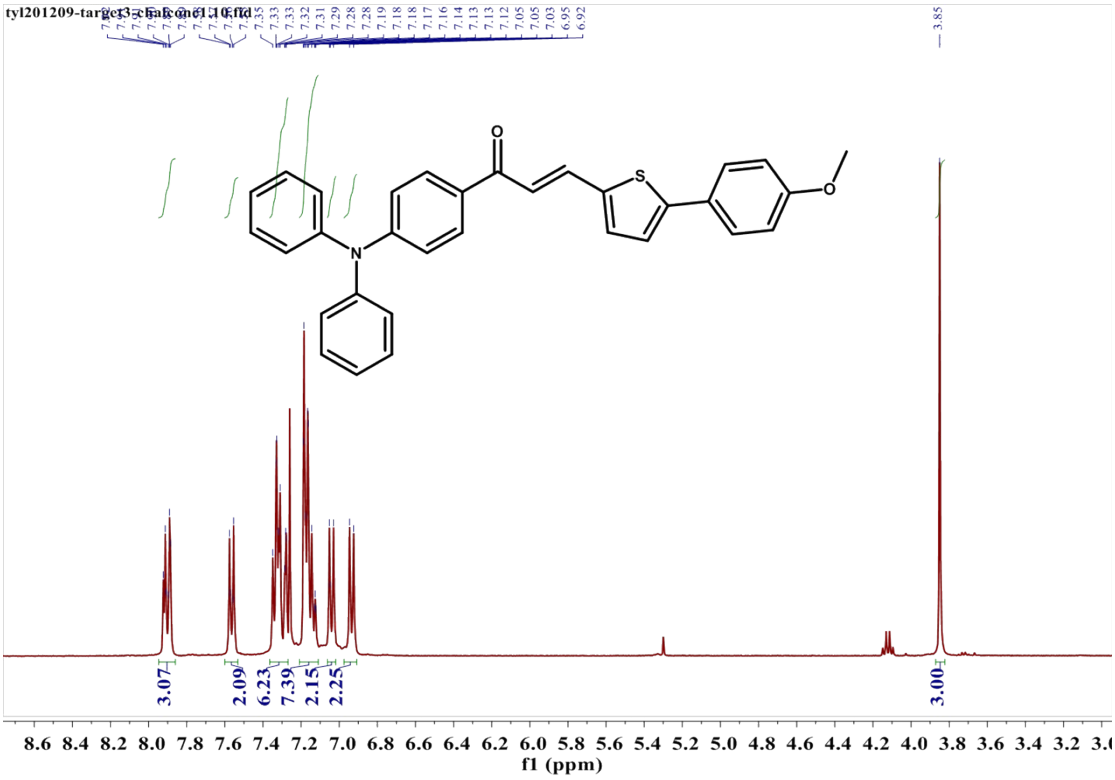

Figure S13. ^{1}H NMR spectrum of 2a in $CDCl_3$

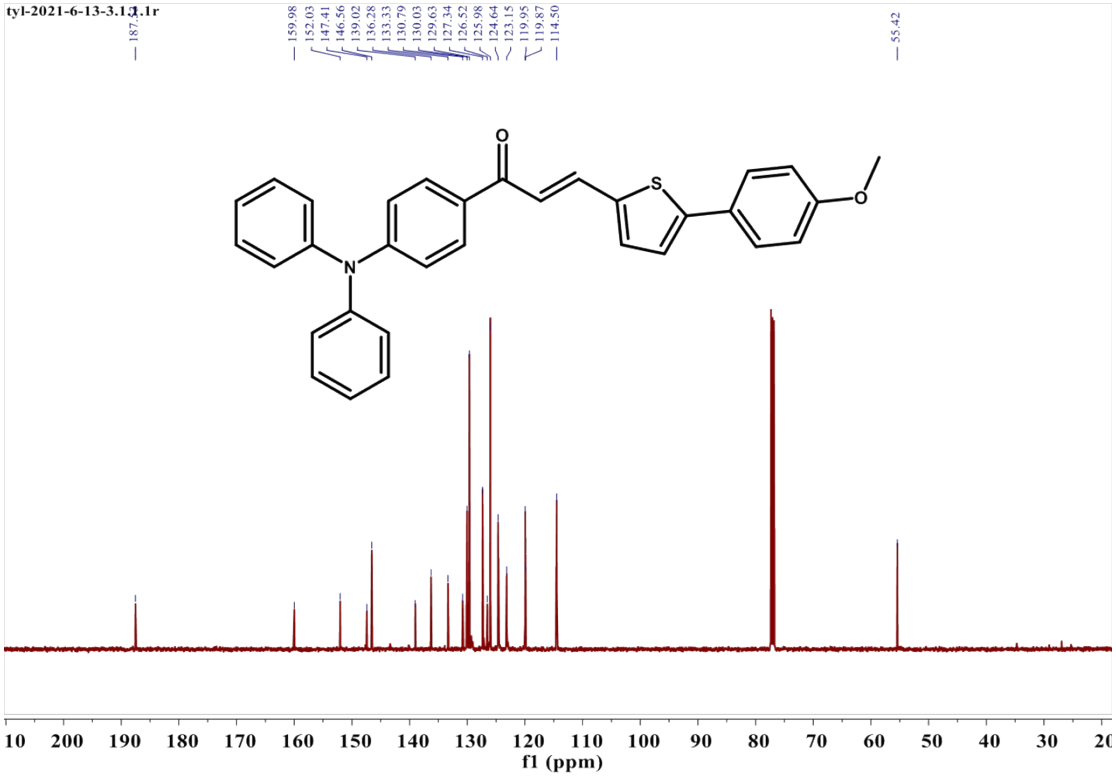

Figure S14. ^{13}C NMR spectrum of 2a in $CDCl_3$.

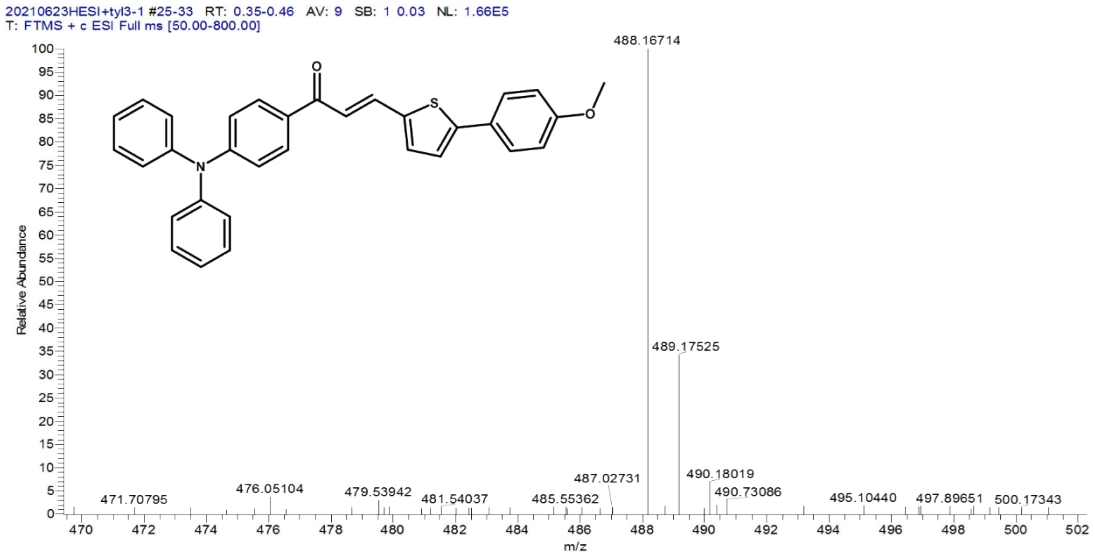

Figure S15. HR-MS spectrum of 2a.

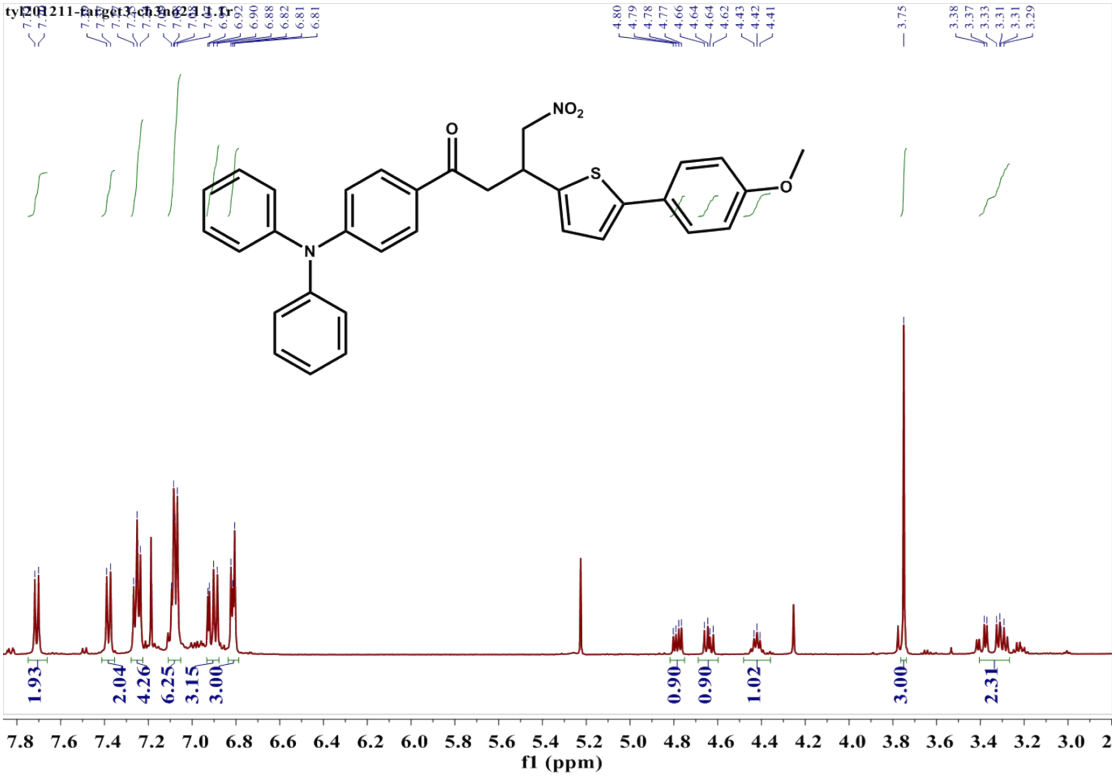

Figure S16. ^{1}H NMR spectrum of 2b in $CDCl_3$.

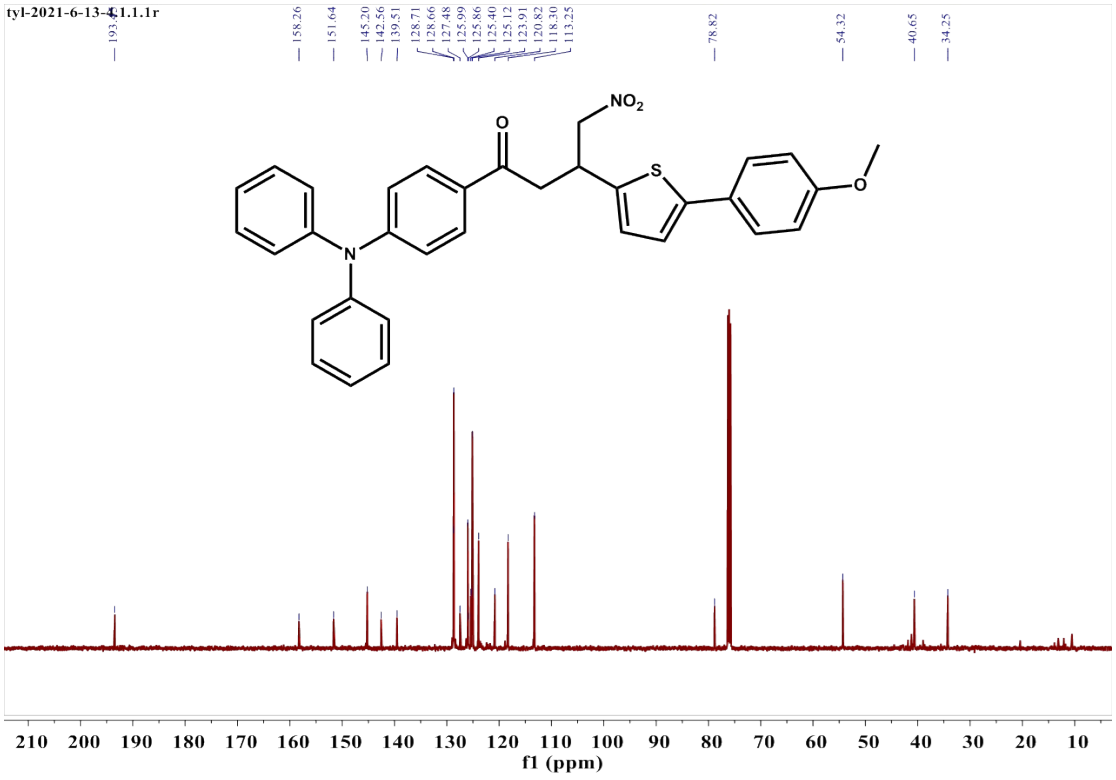

Figure S17. ^{13}C NMR spectrum of 2b in $CDCl_3$.

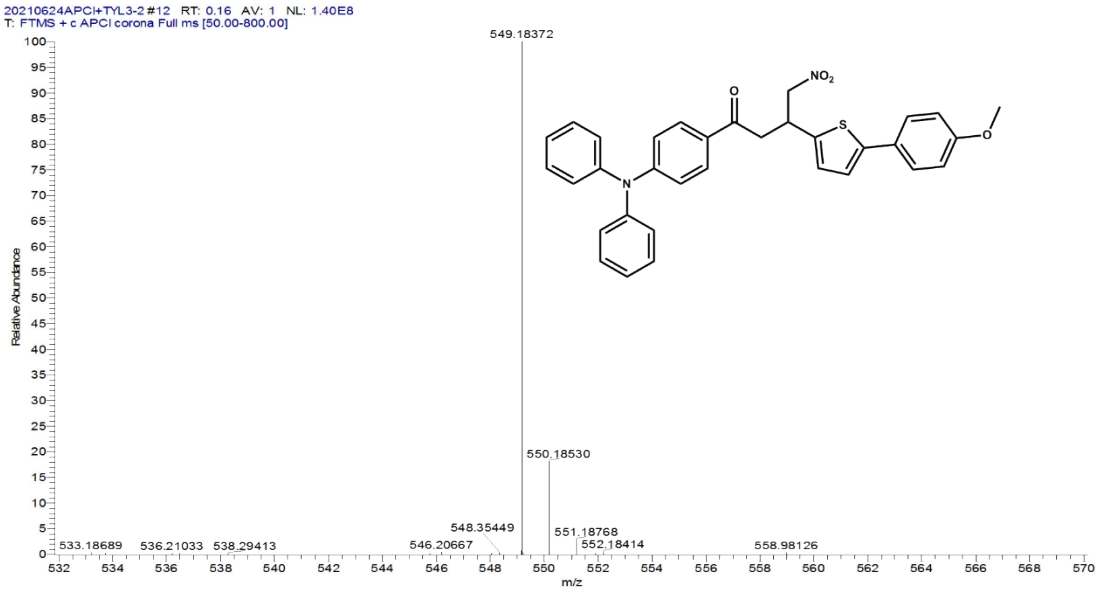

Figure S18. HR-MS spectrum of 2b.

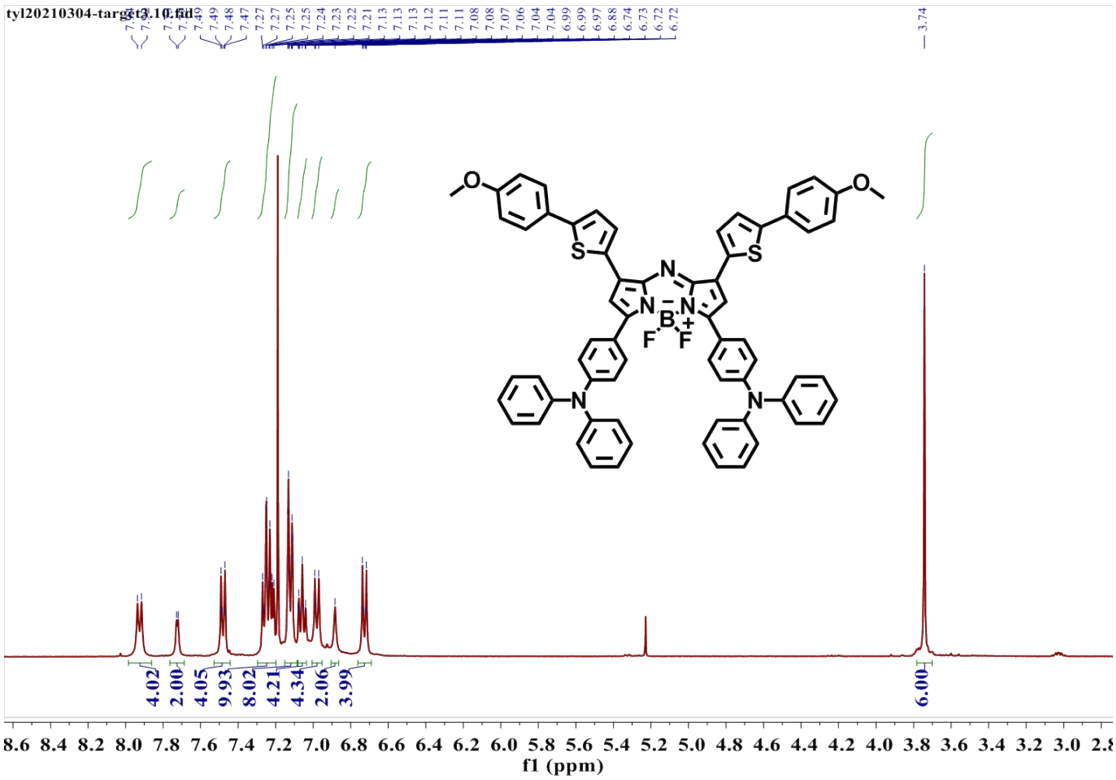

Figure S19. ^{1}H NMR spectrum of dye 2 in $CDCl_3$.

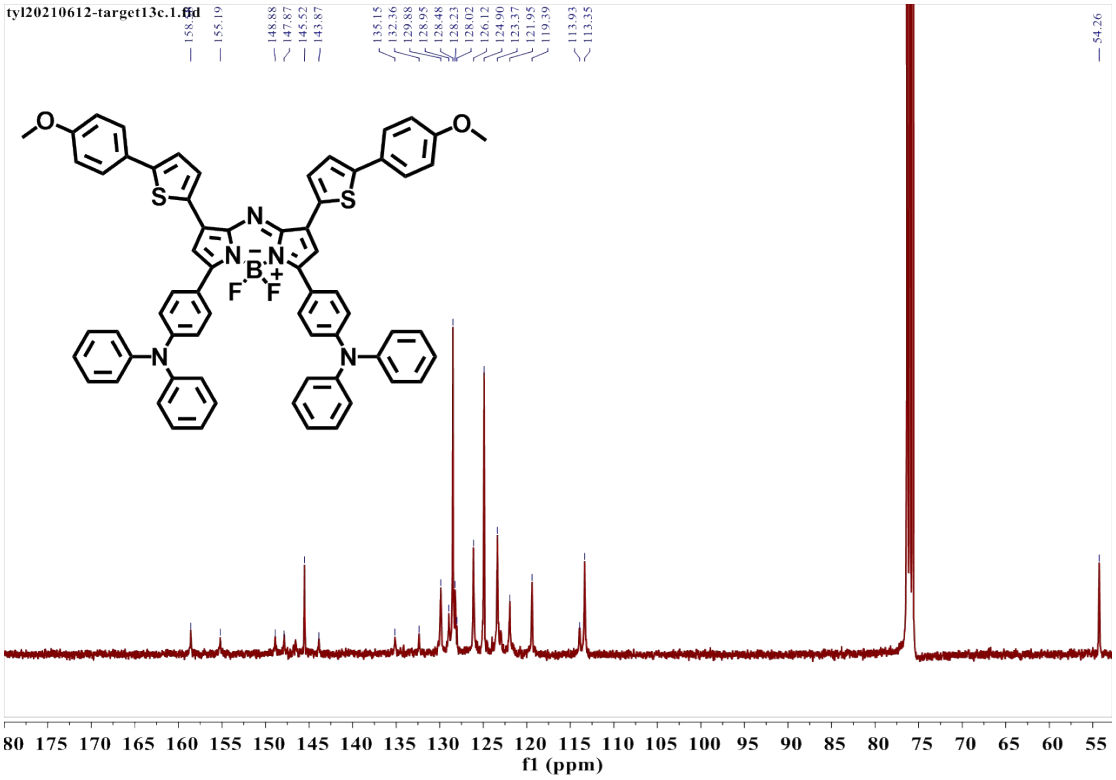

Figure S20. ^{13}C NMR spectrum of dye 2 in $CDCl_3$.

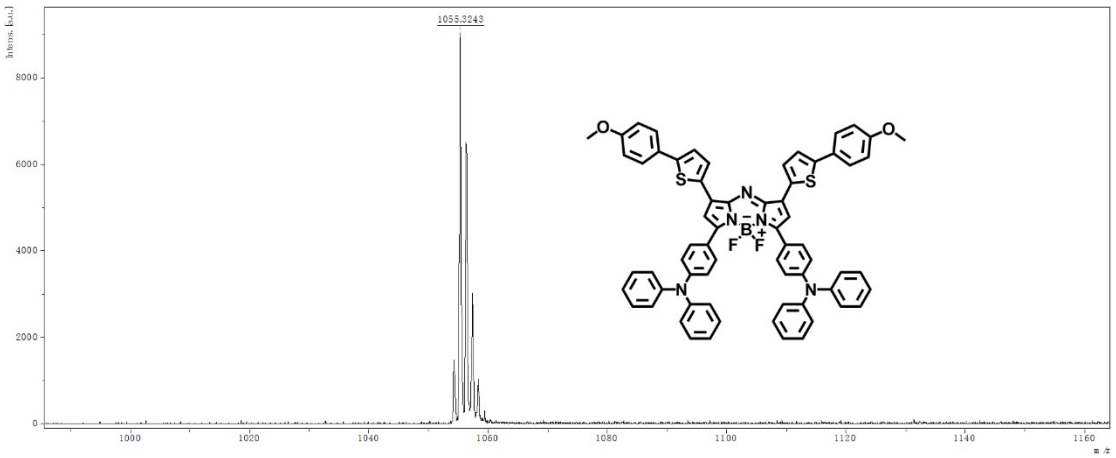

Figure S21. MALDI-TOF-MS spectrum of dye 2.

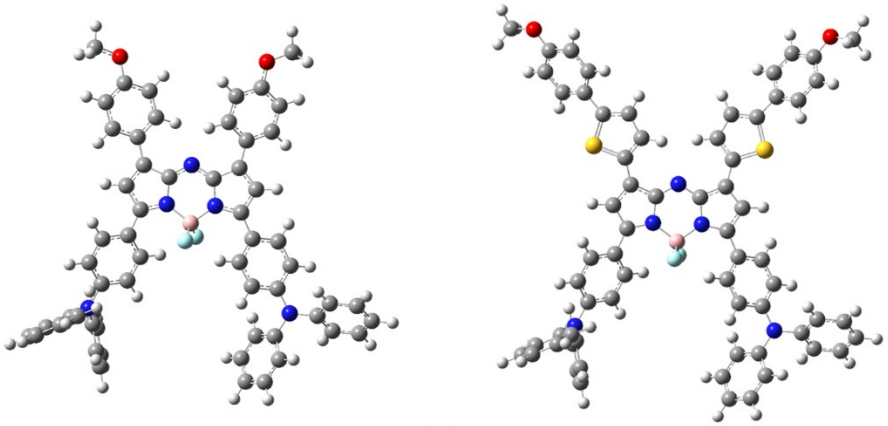

Figure S22. Optimized conformation of dye 1 and dye 2.

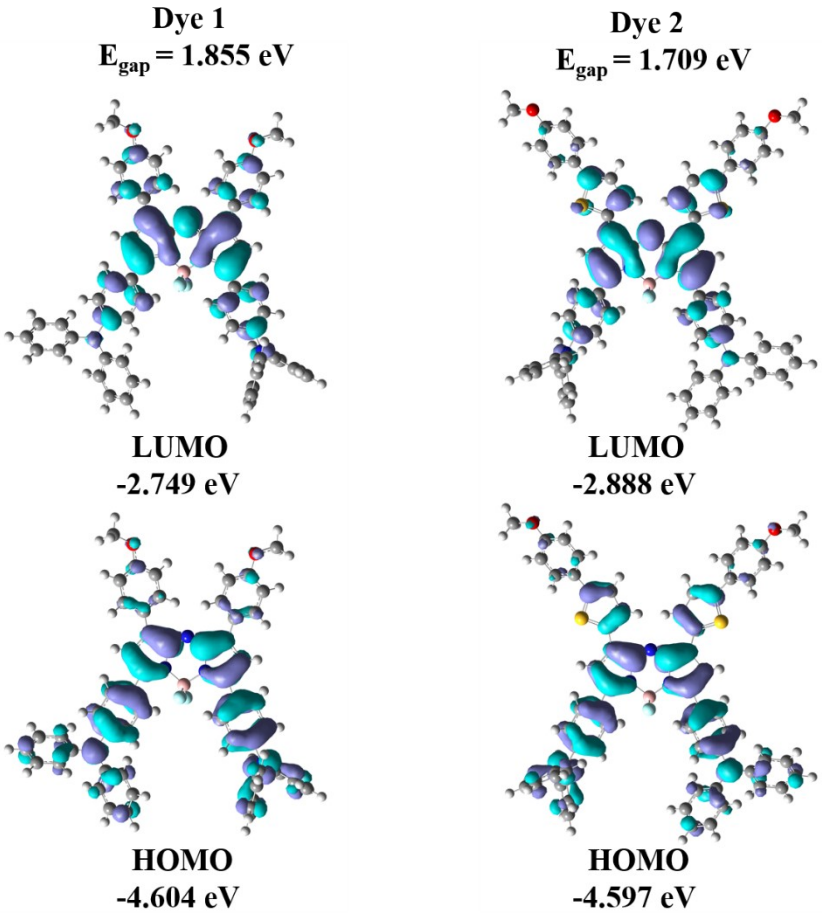

Figure S23. Calculated frontier molecular orbitals for dye 1 and dye 2 and their orbital energies, $E_{gap} = E_{LUMO} - E_{HOMO}$.

Table S1. The optical physical properties of dye 1 and 2.

Dye	Solvent	$\lambda_{abs,\ max}$/nm	ε^a/L•mol^{-1}•cm^{-1}	$\lambda_{em,\ max}$/nm	Stokes shift/nm	Φ^b
1	THF	781	64270	871	90	2.44 %
	NPs (H_2O)	805	54320	N.D.	N.D.	N.D.
2	THF	843	58530	920	77	0.99 %
	NPs (H_2O)	946	39900	1053	107	0.025 %

[a] molar extinction coefficient , [b] absolute fluorescence yield quantum(850-1200 nm)

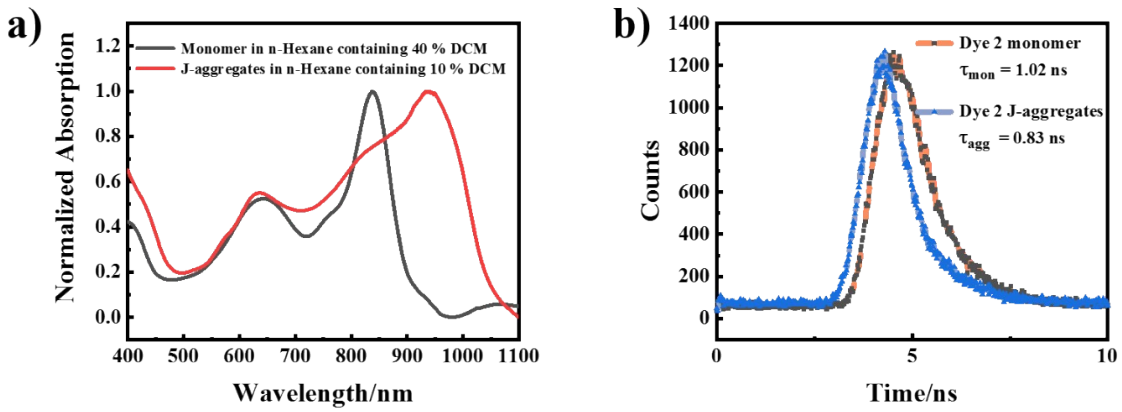

Figure S24. (a) The absorption spectra of dye 2 in n-hexane containing different ratios of DCM. (b) Time-resolved fluorescence decay for dye 2 monomer and J-aggregates in a mixture of n-hexane and DCM.

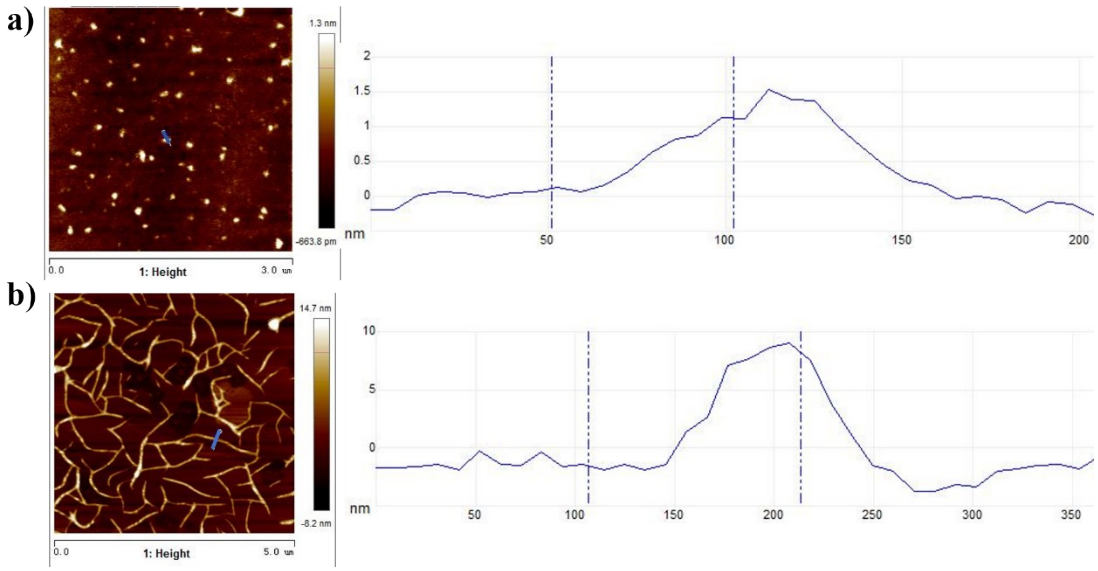

Figure S25. The AFM images height profiles of aggregates of dye 1 (a) and dye 2 (b) with cross-sectional profile along the blue line.

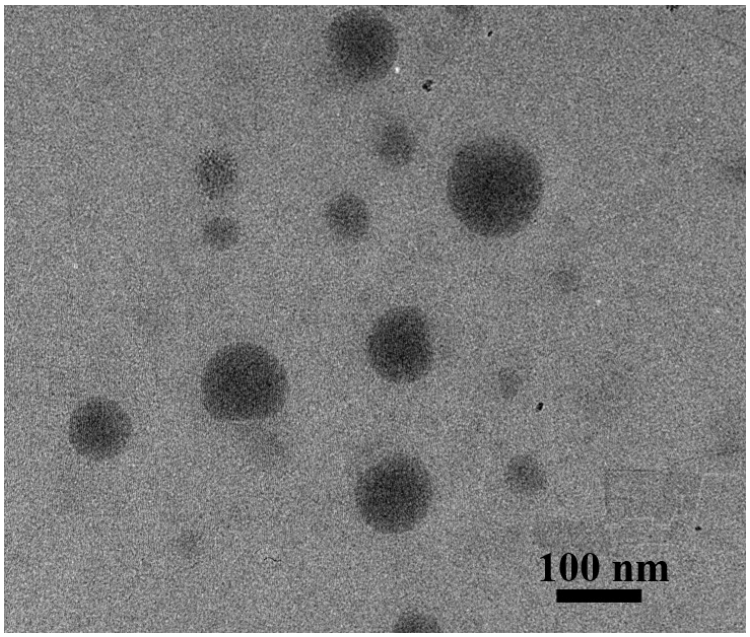

Figure S26. The TEM image of J-NPs.

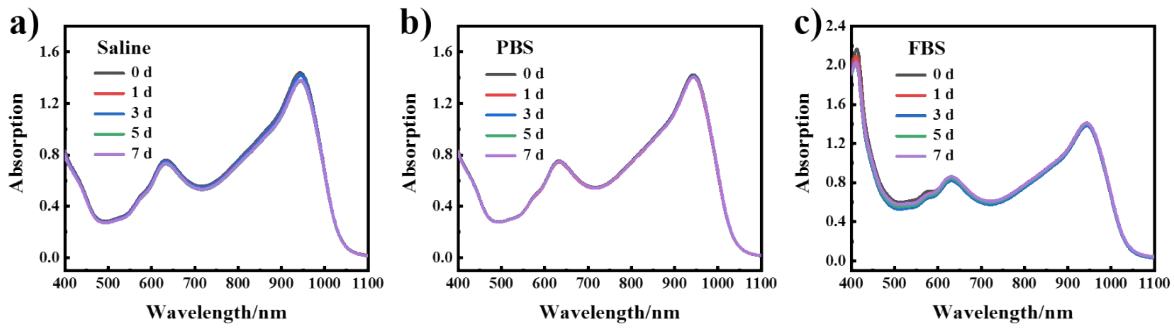

Figure S27. The absorption spectra of J-NPs (30 μM) after incubated with saline, PBS, or FBS for a different time.

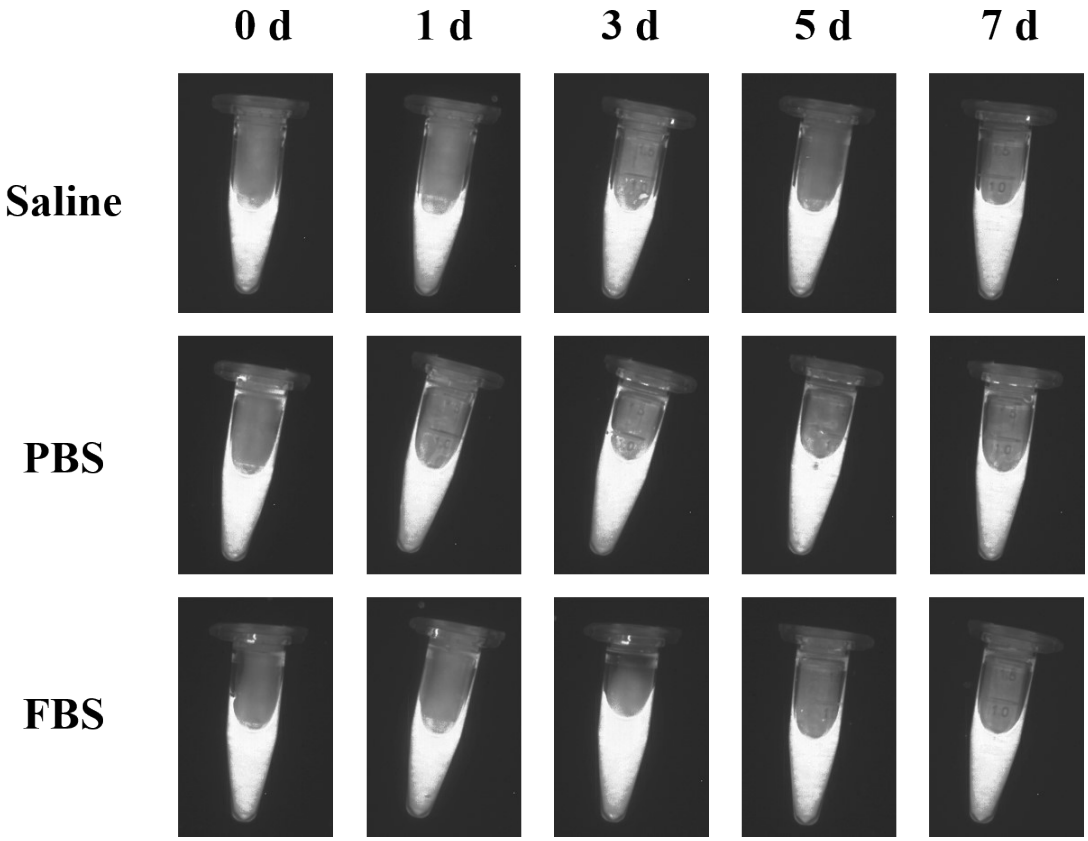

Figure 28. The fluorescence images through a 1000 nm long-wavelength pass filter of J-NPs (30 μM) after incubated with saline, PBS, or FBS for a different time. The number of frame: 10, laser: 808 nm, 50 mW/cm^2.

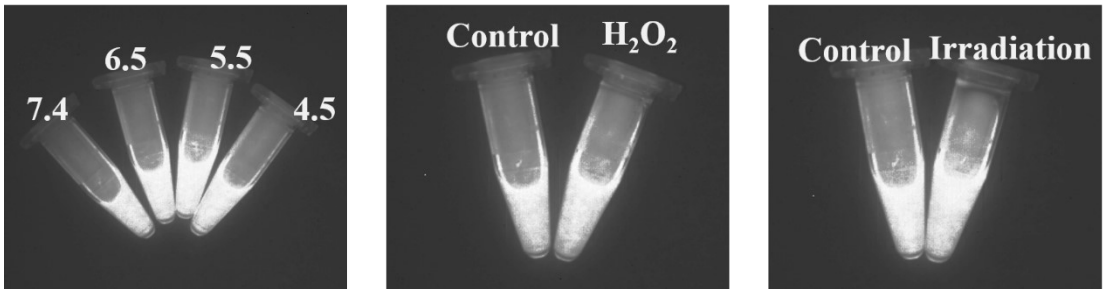

Figure S29. The fluorescence images through a 1000 nm long-wavelength pass filter of dye 2 J-NPs after incubated with different pH value buffer solution and H_2O_2 (200 μM) or exposed to 915 nm laser (1 W/cm^2) for 20 min. The number of frame: 10, concentration: 30 μM, laser: 808 nm, 50 mW/cm^2.

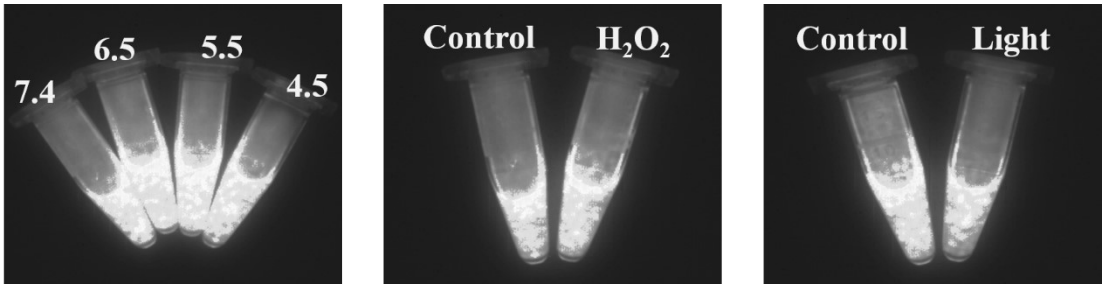

Figure S30. The fluorescence images through a 1000 nm long-wavelength pass filter of dye 2 J-NPs after incubated with different pH value buffer solution and H_2O_2 (200 μM) or exposed to 915 nm laser (1 W/cm^2) for 20 min. The number of frame: 5, concentration: 30 μM, laser: 915 nm, 50 mW/cm^2.

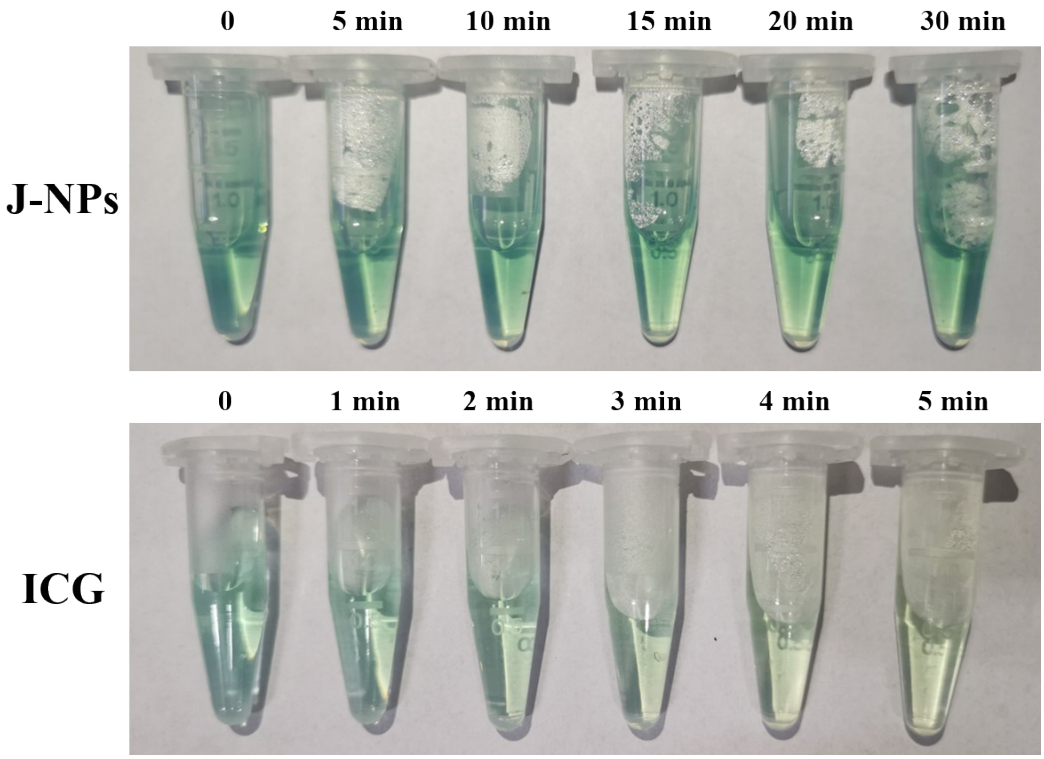

Figure S31. The digital photographs of J-NPs (30 μM) and ICG (10 μM) after exposure to 808 nm irradiation. The power density: 1 W/cm^2 for J-NPs and 0.5 W/cm^2 for ICG.

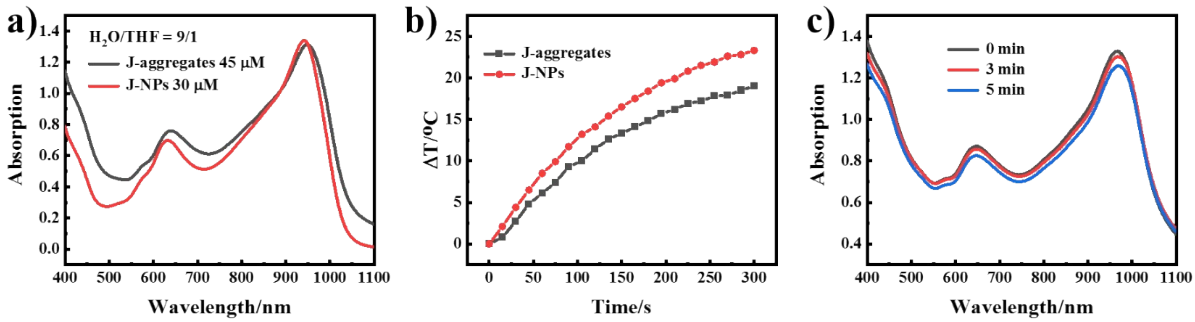

Figure 32. (a) The absorption spectra of J-aggregates and J-NPs and (b) their temperature variation curves under 915 nm irradiation (1 W/cm^{-2}). (c) The absorption spectra of J-aggregates in the mixture of H_2O/THF=9/1 at different times after preparation.

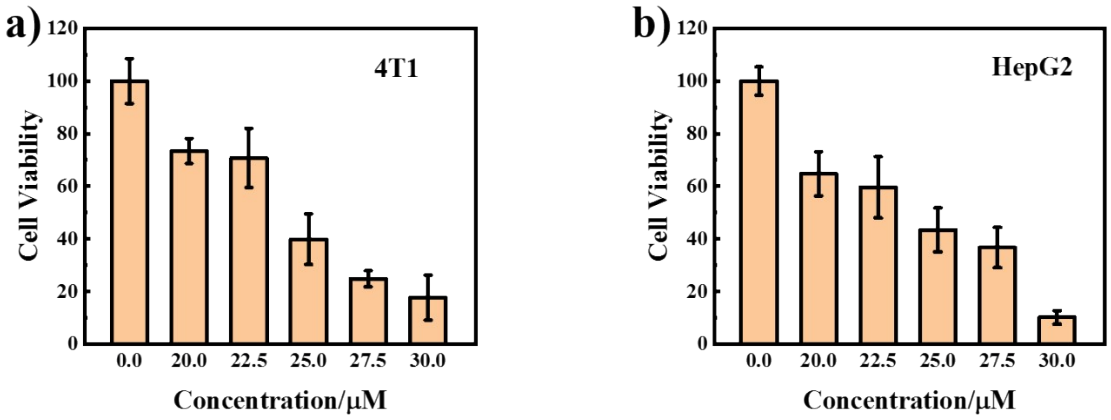

Figure S33. Cell viability of 4T1 (a) and HepG2 (b) cells incubated upon irradiation (915 nm, 1 W/cm^2) in the presence of J-NPs with indicated concentrations (n=4, mean ± SD).

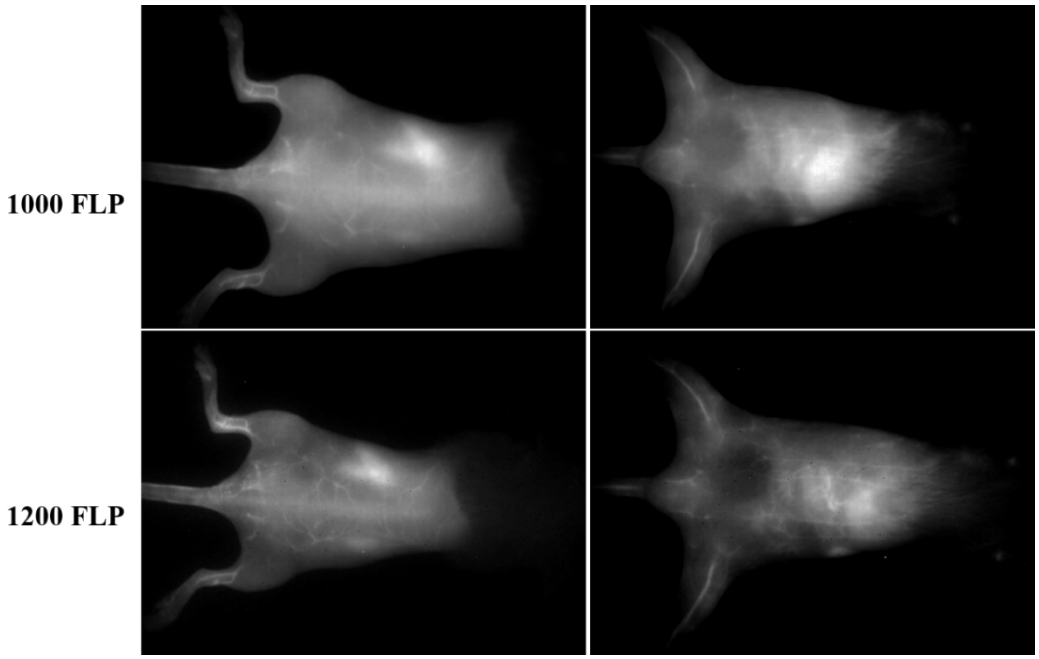

Figure S34. The vascular imaging photographs of mice through different long-wavelength pass filters using J-NPs. The number of frames: 3 for 1000 FLP and 15 for 1200 FLP, excitation light: 915 nm, 50 mW/cm^2.

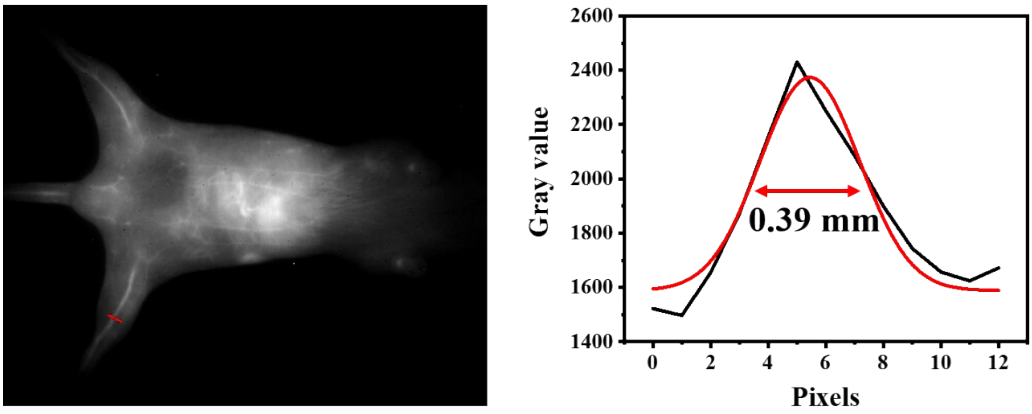

Figure S35. The emission intensity profiles of the red line of interest in left fluorescence photograph (1200 FLP), excitation light: 915 nm, 50 mW/cm^2..

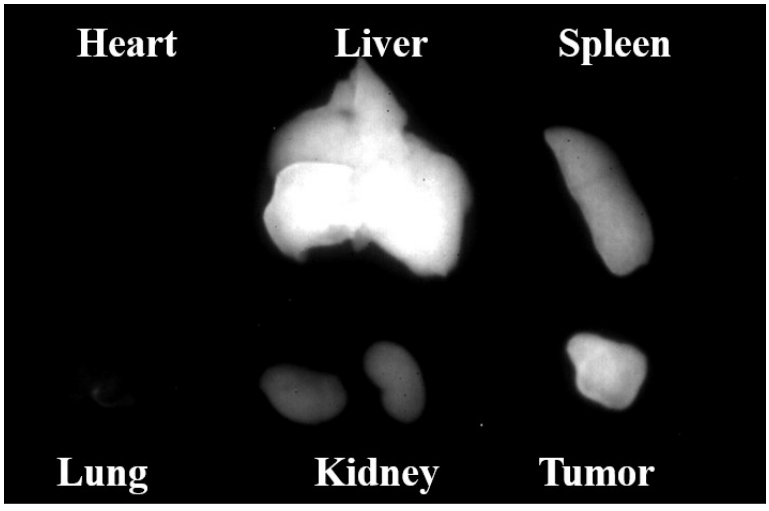

Figure S36. The *ex vivo* biodistribution of J-NPs in main organs and tumor after 72 h post-injection under 808 nm laser excitation, 50 mW/cm^2. The number of frames: 14.

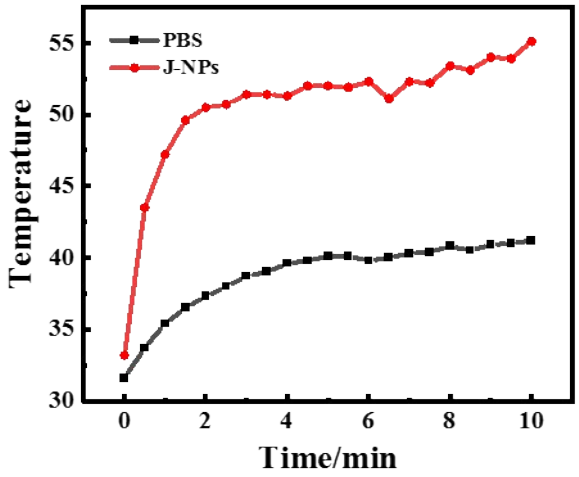

Figure S37. The temperature variation on the tumor during the 915 nm irradiation process.

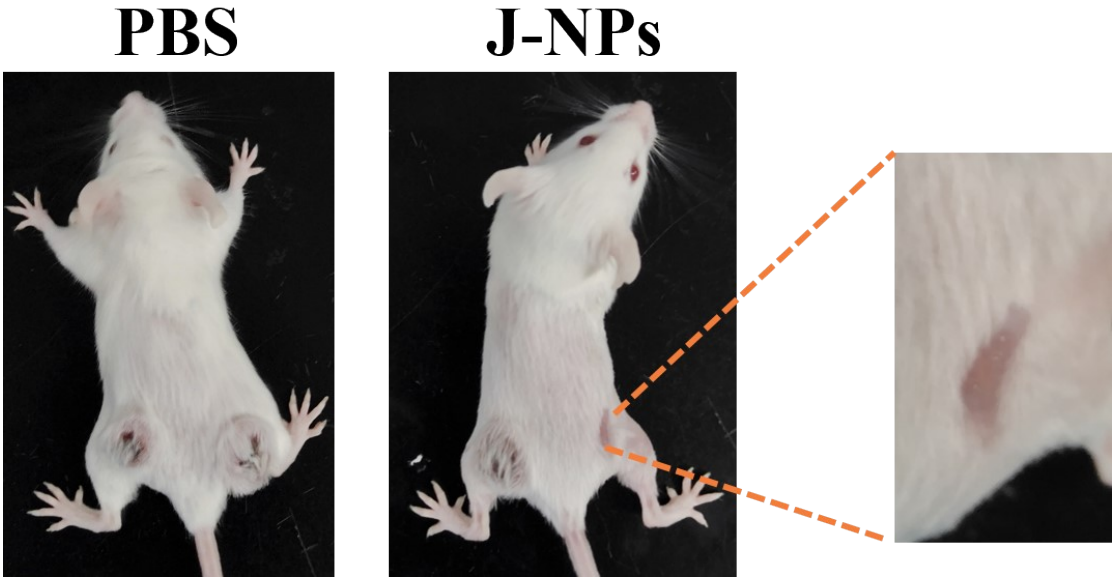

Figure S38. The digital photographs of mice after 21 days of treatment.

References

1. A. Frisch, Gaussian 09, Revision E.01, Gaussian Inc., Wallingford CT, USA, 2009.
2. L. Liu, L. Fu, T. Jing, Z. Ruan and L. Yan, *Acs Appl. Mater. & Interfaces*, 2016, **8**, 8980-8990.
3. T. Li, L. Liu, T. Jing, Z. Ruan, P. Yuan and L. Yan, *ACS Appl. Mater. & Interfaces*, 2018, **10**, 14517-14530.
4. D. Xi, M. Xiao, J. Cao, L. Zhao, N. Xu, S. Long, J. Fan, K. Shao, W. Sun, X. Yan and X. Peng, *Adv. Mater.*, 2020, **32**, e1907855.